WESTERN PACIFIC EARTH SCIENCES
Vol.1, No.4, P.443-458, 7 Figs., 2 Tabs., November, 2001

ASTRONOMICALLY TUNED LATE PLIOCENE-PLEISTOCENE BENTHIC $\delta^{18}O$ CHRONOSTRATIGRAPHY FOR THE SUBTROPICAL WESTERN PACIFIC AND ITS PALEOCLIMATIC SIGNIFICANCE

MENG-YANG LEE[1,2], KUO-YEN WEI[1] AND YUE-GAU CHEN[1]

1. Department of Geosciences, National Taiwan University, Taipei, Taiwan, R.O.C.
2. Current address: Institute of Earth Sciences, Academia Sinica, Taipei, Taiwan, R.O.C.

ABSTRACT

High-resolution benthic oxygen isotope record from Core MD972143 has been calibrated to extend the astronomical timescale back to 2.2 Ma for the western Pacific Ocean. All oxygen isotope stages down to Stage 83 were recognized and validated by comparison with the magnetostratigraphy of the same core of Horng (2000). The astronomical timescale of Core MD972143 was constructed by correlating the $\delta^{18}O$ record to the low-latitude stack timescale of Bassinot *et al.* (1994) for the past 0.9 Ma and to the astronomical timescale of ODP Site 677 of Shackleton *et al.* (1990) for the period of 0.9-2.2 Ma. The resultant $\delta^{18}O$ time series reveals global ice-volume variability in both time and frequency domains.

Spectral analyses and filtering of the calibrated time-series reveals the evolutive nature of the respective 41-kyr and 100-kyr components through the past 2.2 Ma. In contrast to the constancy of the 41-kyr response in the record, the amplitude of the filtered 100-kyr band exhibits characteristics worthwhile for further examination. High-amplitude of 100-kyr periodicity appeared initially at about 1.2 Ma and remained stable until about 0.9 Ma. After that, the 100-kyr component began to predominate and accentuated eventually to its full dominance at ~400 ka. The results suggest that the occurrence and evolution of the 100-kyr cycles went through multi-step transitions. The mid-Pleistocene revolution is characterized by the increase of 100-kyr cyclicity over the ever-lasting 41-kyr component, and an increase in amplitude of global ice volume fluctuation.

Key words: chronology, oxygen isotope, Milankovitch cycles, Quaternary

INTRODUCTION

Variations in the Earth's orbital geometry are responsible for the seasonal distribution of incoming solar insolation and, hence, the timing of climatic oscillations in the geological past. The imprint of orbitally forced glacial-interglacial fluctuations on geological record has been well documented since the late 1970s (e.g. Hays *et al.*, 1976; Imbrie *et al.*, 1984; Hagelberg *et al.*, 1991; Imbrie *et al.*, 1992, 1993). This has led to the development of high-resolution astronomical timescales throughout the late Neogene by tuning paleoclimatic indicators to the astronomical forcing functions (Imbrie *et al.*, 1984; Martinson *et al.*, 1987; Ruddiman *et al.*, 1986, 1989; Raymo *et al.*, 1989; Shackleton *et al.*, 1990, 1995). In a landmark paper, Shackleton *et al.* (1990) proposed a revised astronomical calibration of the lower Pleistocene timescale based upon oxygen isotope profile of ODP Site 677, which yields estimated ages for geomagnetic reversals that are systematically 5-7% older than previous radiometric dates (Mankinen and Dalrymple, 1979). These revised ages of the polarity reversals have since been confirmed by the advanced $^{40}Ar/^{39}Ar$ dating technique (e.g. Baksi *et al.*, 1992; Spell and McDougall, 1992; see also review by Kent, 1999). With a potential accuracy and resolution of a few thousand years, orbital tuning of oxygen isotope records provides a more precise timescale than is obtainable by any other means.

Properties of the deep Pacific Ocean water, blessed by its great mass and uniformity, are advantageous to serve as a reference base to represent the global ocean mean state in paleoceanography research (Shackleton *et al.*, 1983; Curry and Crowley, 1987). Considerable evidence exists that substantial changes of deep Pacific waters took place on glacial-interglacial timescale during the late Pleistocene (Curry *et al.*, 1988; Herguera *et al.*, 1992; Ohkouchi *et al.*, 1994; Keigwin, 1998). The relatively short record lengths of most paleoclimatic time series of the western Pacific, however, have precluded the assessment of long-term evolution of Milankovitch cyclicity through the late Neogene. One of the best records of Quaternary glacial-interglacial fluctuations is found on the Ontong Java Plateau in the western equatorial Pacific. Two piston cores from the plateau (V28-238 and V28-239) have long provided a standard chronology for the late Pleistocene (Shackleton and Opdyke, 1973, 1976). More recently, a planktonic oxygen isotope record of Site 806 from Ocean Drilling Program Leg 130 was calibrated by matching the variations to an orbital template and established an astronomical timescale back to 2 Ma (Berger *et al.*, 1994). Note that these records are disturbed as a result of coring problems such as core breaks (e.g. ODP Site 806 core 1/2 = 0.16m, core 2/3 = 0.74m, Berger *et al.*, 1993), and/or of pervasive carbonate dissolution at the depths from which the cores were raised (Wu *et al.*, 1990). It is not absolutely certain whether such a composite record is complete and therefore permits an accurate astronomical calibration.

In this study we present a high-resolution benthic oxygen isotope record to extend the astronomical timescale for the western Pacific Ocean back to 2.2 Ma. In comparison with the detailed magnetostratigraphy of the same core (Horng, 2000), we recognized all the oxygen isotope stages down to Stages 83 and developed an age model by correlating our $\delta^{18}O$ record to previous published astronomical timescales. On the basis of the calibrated time series, we evaluated the changes of dominant Milankovitch periodicities in the long-term geological record, especially on the nature of the middle Pleistocene climate transition.

MATERIALS AND METHODS

Due to the deep bathymetry and shallow carbonate compensation depth (CCD) of the western Pacific Ocean, there is virtually no long record for documenting the paleoceanographic variability of the subtropical Pacific. Cores drilled by the Deep Sea Drilling Project Leg 31 in the West Philippine Sea provides only low-quality, fragmented sequences and have never been amenable for paleoceanographic studies. During Leg II of the IMAGES III Cruise in June 1997, as a return visit to the DSDP Site 292, Core MD972143 (15°52.26' N, 124°38.96'E) was retrieved at a water depth of 2989m on the Benham Rise in the West Philippine Sea (Fig. 1). Intercalated conspicuously in the 38-meter sequence of hemi-pelagic calcareous ooze are 12 distinct volcanic ash layers, of which the thickness ranges from 1cm to 16cm. A layer of carbonate turbidite at subdepth 32.95m to 33.95m, consisting mainly of coral fragments and foraminifera, appears to truncate the sequence and probably results in a hiatus. This turbidite layer containing sediments with median size coarser than 150μm might originate from the eastern shoaler region of the Benham Bank. The age of the lowermost part of the core is constrained by calcareous nannofossil biostratigrapy and is older than 2.59 Ma but younger than 2.78 Ma (Wei *et al.*, 1998).

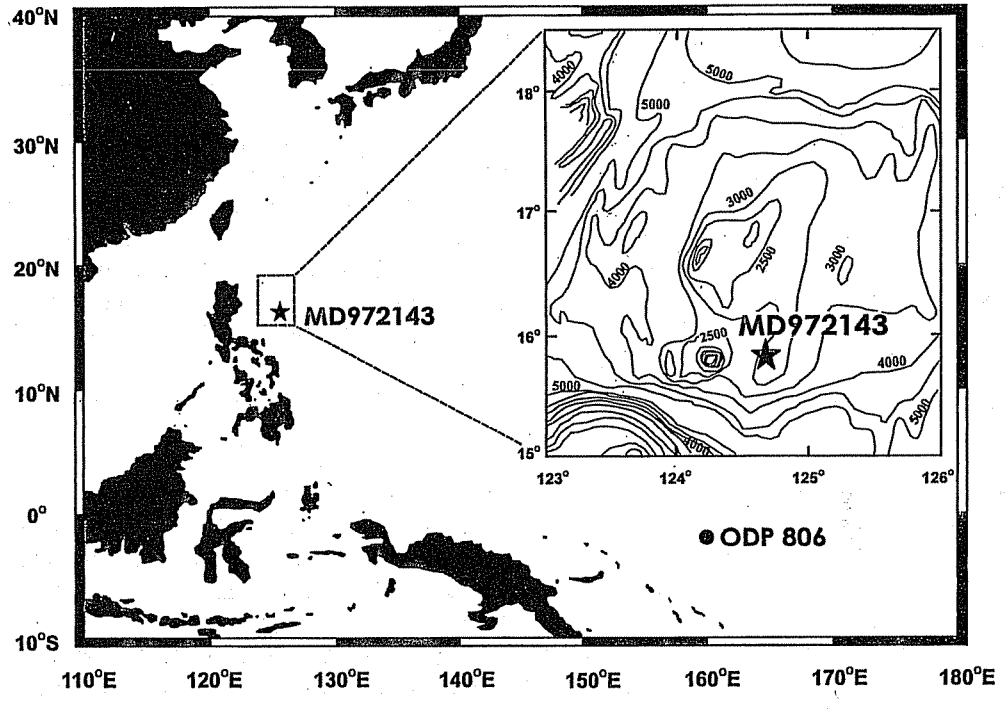

Figure 1. Locations of Core MD972143 (15°52.3' N, 124°39.0'E, 2989m) and ODP Site 806 (0°19.1' N, 159° 21.7'E, 2520m) in the western Pacific Ocean. The detailed bathymetry of the Benham Rise is shown in the inset map (modified from Ingle *et al.*, 1975). The numbers inserted in contour lines represent water depth in meters.

Samples were taken every 4cm throughout the core to yield an average sampling resolution of 1-4 kyr. A total of 799 levels were selected to perform oxygen stable isotope analysis. The temporal resolution for the late Pleistocene is about 2 kyr per sample, while that for the early Pleistocene to Pliocene is about 4 kyr per sample. Although the site is located well above the present depth of the foraminifer lysocline in this region (~3400 m; Berger and Johnson, 1976; Berger *et al.*, 1982), the dissolution-susceptible planktonic foraminifers (e.g. *Globigerinoides sacculifer* and *Globigerinoides ruber*) were strongly affected by differential dissolution at many intervals. Specimens of an epibenthic foraminifer species, *Cibicidoides wuellerstorfi*, were picked from the size fraction larger than 150μm for isotopic analysis. The picked specimens were cleaned twice by ultrasonic vibration for 5-10 seconds to remove adhering fine particles. Samples were then treated with NaClO (5%) at room temperature for 24 hours to remove organic matter. Isotope measurements were performed on a Finnegan Delta Plus mass spectrometer with an automated carbonate device at the Department of Geosciences, National Taiwan University. Average values from the duplicated or triplicated results were reported with respect to the PDB standard through calibration against the routinely analyzed National Bureau of Standards (NBS) 19 with a precision of 0.08‰.

RESULTS AND DISCUSSIONS

Oxygen Isotope Stratigraphy of Core MD972143

Core MD972143 provides for the first time a continuous, high-resolution benthic oxygen isotope record from the late Pliocene to the present in the western subtropical Pacific. All oxygen isotope stages down to Stage 83 (~33m), as defined by Emiliani (1955), Shackleton and Opdyke (1973) and Ruddiman *et al.* (1986), were recognized and indicated in Figure 2. In such a scheme, stages are numbered consecutively from the top of the record downward, with odd numbered stages corresponding to interglacial intervals and even numbers corresponding to glacial intervals. Several characteristic isotopic architectures were easily recognized in Core MD972143, such as the significantly prolonged interglacial Stage 35 and the less developed glaciations during Stages 27/29, Stages 55/57 and Stages 65/69. For the uppermost 17m of Core MD972143, oxygen isotopic events were further labeled on the detailed $\delta^{18}O$ record, adopting the revised numbering of the low-latitude oxygen isotope stack (Bassinot *et al.*, 1994).

The assignment of marine isotope stages was validated by a comparison with the high-quality magnetostratigraphy of the same core published by Horng (2000). Three prominent normal-polarity zones were identified by Horng (2000): the Brunhes (0-1560 cm), Jaramillo (1823-1905 cm) and Olduvai (2738-2937 cm). Below the Brunhes/Matuyama geomagnetic reversal boundary, Australasian microtektites were found at the depths of 1527-1595cm with the peak abundance at 1571cm (Lee and Wei, 2000). The stratigraphic occurrence of Australasian microtektites, centered at oxygen isotope Stage 20 (Smit *et al.*, 1991; Schneider *et al.*, 1992; Jian *et al.*, 2000), can serve as an independent isochronous marker for regional correlation (Lee and Wei, 2000). In addition, four short normal-polarity events within the Matuyama Chron were detected at the intervals of 1728-1735 cm (Kamikatura), 2031-2044 cm (Cobb Mountain), 3231-3270 cm (Réunions II) and 3295-3305 cm (Réunions I) (Horng, 2000). The Kamikatura event, previously assigned as Santa Rosa event in Horng (2000), was re-evaluated and designated based upon its stratigraphic position in our newly generated oxygen isotope timescale. The identification of Réunions I remains uncertain as the normal-polarity interval is located within

the carbonate turbidite layer and the directions of characteristic remanent magnetization are scattered. The stratigraphic positions of magnetic reversals in terms of oxygen isotope stages are listed in Table 1. Our results are in good agreement with the recent chronostratigraphic compilation by Berggren *et al.* (1995).

According to the calcareous nannofossil biostratigraphy, the age of the lowermost part of the core is older than 2.59 Ma (LAD of *Discoaster surculus*) but younger than 2.78 Ma (LAD of *Discoster tamalis*) (Wei *et al.*, 1998). On the other hand, the age of the lowermost section of the core (34-38m) can also be constrained as being older than the Réunions II (~2.14 Ma, Berggren *et al.*, 1995) and younger than the Matuyama/Gauss reversal (2.58 Ma, Berggren *et al.*, 1995), since the magnetic polarity remains at reversed directions (Horng, 2000). This inconsistency between bio- and magneto- stratigraphy demands further work to clarify the discrepancy among these two approaches. In this paper, the $\delta^{18}O$ data below 32.9m (carbonate turbidite layer) will not be discussed given the uncertainty of their absolute ages.

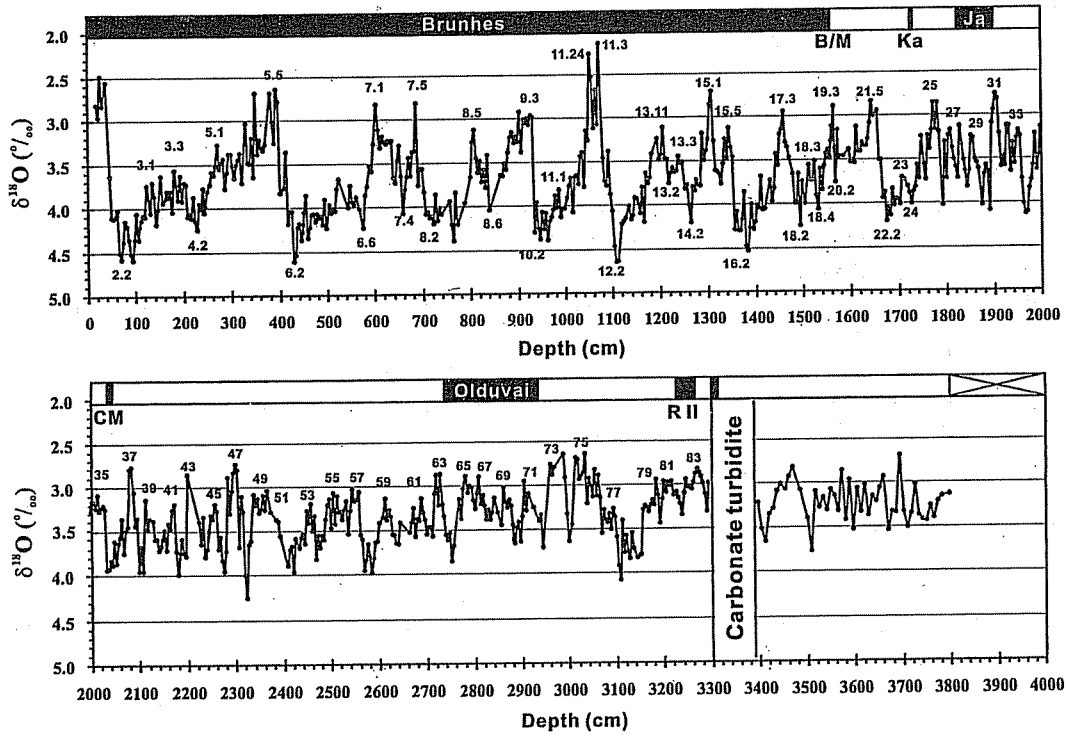

Figure 2. Oxygen isotope stratigraphy and magnetostratigraphy of Core MD972143. Digital numbers represent various oxygen isotopic events down to Stage 83, referable to the low-latitude stack of Bassinot *et al.* (1994) and oxygen isotope stratigraphy of the Site 677 of Shackleton *et al.* (1990). A layer of carbonate turbidite occurs at subdepth 32.95m to 33.95m. The upper bar shows the magnetic polarity pattern constructed by Horng (2000). Ja, Ka, CM, and RII refer to Jaramillo subchron, and Kamikatura, Cobb Mountain and Réunions II events, respectively.

Table 1. Magnetic reversals correlated with marine oxygen isotope stages (MIS) in Core MD972143.

Magnetic Reversal	MIS
Brunhes/Matuyama	19
Kamikatura	24
Top of Jaramillio	27
Base of Jaramillo	31
Cobb Mountain	35
Top of Olduvai	63
Base of Olduvai	71
Reunions II	82

Astronomical Timescale for Core MD972143

The age model for Core MD972143 was developed by correlating the benthic $\delta^{18}O$ record to the low-latitude stack timescale of Bassinot *et al.* (1994) for the past 900 kyr and the rest of the record to the fine tuned astronomical timescale of Site 677 of Shackleton *et al.* (1990). Both of the two previously published timescales chose the Imbrie and Imbrie (1980) nonlinear ice model as their tuning target, which promises an internal consistency among these resultant astronomical timescales. The model assumes that the rate of climate response (growth or decay of northern hemispheric ice sheets) is proportional to the magnitude of the summer insolation forcing at 65°N. The target curve was constructed using the monthly insolation series for July at 65°N of Berger and Loutre (1991). By aligning features in the $\delta^{18}O$ record of Core MD972143 with features in these two orbitally tuned oxygen isotope curves, we designated age controlling points to construct the age model for Core MD972143 (Tab. 2). It should be noted that we developed our astronomical age model after subtracting the thickness of tephra layers from the original sedimentary sequence. The age of each sample was then estimated by linear interpolation between the controlling points by assuming uniform accumulation between the anchor points.

We performed a series of cross-spectral analyses to optimize the match between our data set and the reference curve. Age models were improved stepwise by adding and deleting age-controlling points to maximize the coherency of the two time-series at the major Milankovitch orbital bands, namely precession (~21 kyr), obliquity (~41 kyr) and eccentricity (~100 kyr) (Fig. 3a). Our objective in performing cross-spectral analysis against the ODP Site 677 record over the past 2.2 Myr, rather than against the individual curve, is purely one of convenience to obtain a compact summary of orbital-isotopic relationships across the entire visible spectrum in a single diagram. We followed the standard techniques described in Imbrie *et al.* (1992) using the ARAND package provided by P.J. Howell of Brown University. The final result shows that the two $\delta^{18}O$ time series are highly coherent, reaching coherency larger than 0.95 at the three

major orbital frequencies. These values are well above the non-zero coherency value at the confidence level of 95%. The spectral power is higher at obliquity and eccentricity cycles, whereas the spectral variance at precession cycle is lower in Core MD972143. In addition, the phase spectra provide another criteria to evaluate our final age model. In the record studied here, the phase angles are tuned to zero degree (in phase) at the Milankovitch frequency bands (Fig. 3b).

Table 2. Control points used for depth-to-age conversion in Core MD972143.

Depth (cm)	Age (ka)	Depth(cm)	Age(ka)	Depth (cm)	Age (ka)	Depth (cm)	Age (ka)
37	8	1263	536	2027	1195	2688	1736
69	17	1307	573	2031	1207	2712	1757
123	30	1343	615	2083	1242	2728	1775
181	52	1363	628	2100	1249	2752	1795
229	62	1459	688	2112	1279	2780	1807
269	79	1495	718	2144	1286	2840	1866
393	122	1515	729	2172	1316	2856	1881
429	133	1531	754	2180	1334	2868	1896
575	174	1563	782	2200	1351	2884	1910
603	194	1567	793	2236	1376	2904	1940
659	225	1655	858	2256	1404	2944	1955
687	236	1675	871	2276	1422	2988	1984
715	248	1707	905	2304	1453	3000	1992
807	287	1727	918	2324	1460	3032	2021
839	295	1779	956	2336	1471	3092	2072
931	328	1791	965	2364	1490	3108	2079
935	340	1807	977	2420	1537	3152	2096
987	369	1827	997	2456	1560	3184	2119
1039	390	1855	1026	2468	1572	3192	2129
1071	406	1875	1036	2556	1641	3236	2153
1107	434	1903	1073	2568	1649	3268	2187
1195	481	1955	1115	2612	1684	3288	2193
1219	510	1971	1129	2640	1702		
1239	524	1999	1143	2672	1716		

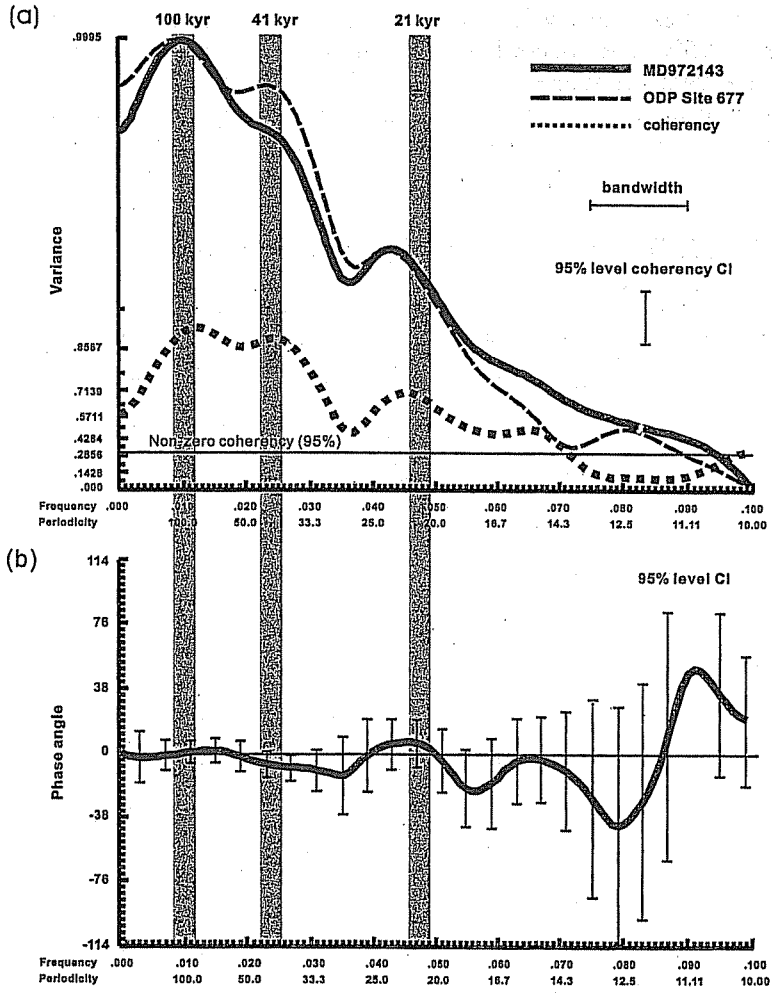

Figure 3. Cross-spectral analysis (a) and phase spectra (b) between oxygen isotope time series of Core MD972143 and ODP Site 677. The isotopic record was sampled at a constant 2-kyrs time-interval and then linearly detrended before spectral analysis.

The depth vs. age plot of Core MD972143 shows rather good linear relationship among three sections (Fig. 4). Based on the depth-age pairs, the average sedimentation rates of various intervals were calculated as follows: ~4 cm/kyr for the topmost 5 meters, ~2 cm/kyr for the interval between 5 and 12 meters, and ~1.2 cm/kyr for the interval between 12 and 32 meters. The apparent high sedimentation rate of the uppermost section is mainly an artifact caused by the stretching of the sedimentary column during piston coring, and due to the high water content of loosely compacted sediments.One should be cautious in interpreting changes of mass accumulation rates derived from the sedimentation rate, such as the secular variation of carbonate productivity over the last few glacial-interglacial cycles.

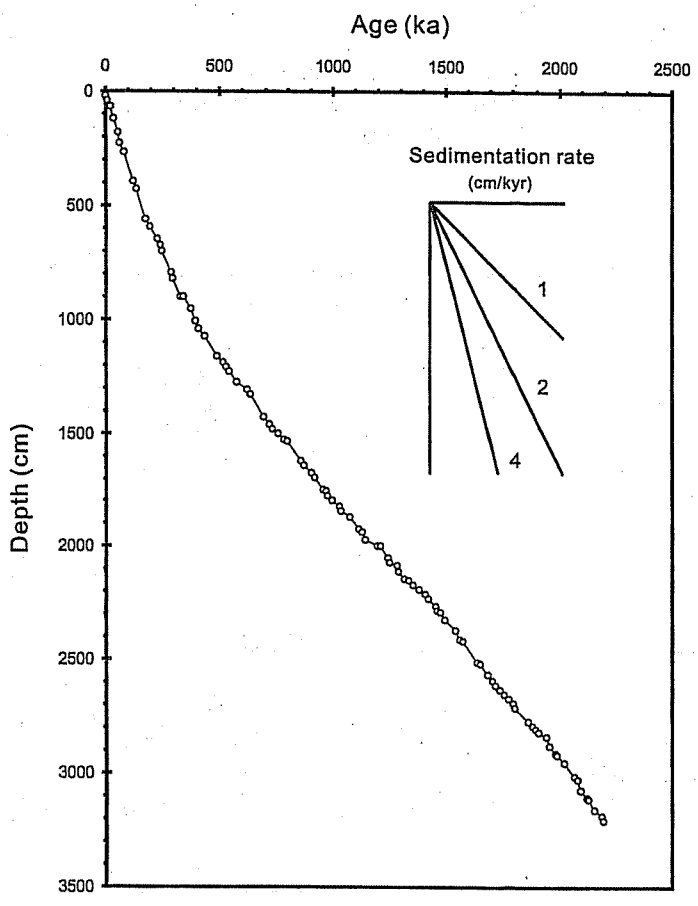

Figure 4. Depth-age plot of age controlling points in Core MD972143 based on the timescales of Bassinot *et al.* (1994) for the past 0.9 Ma and Shackleton *et al.* (1990) for the 0.9-2.2 Ma.

Comparisons with Other Published Astronomical Timescales

The ages for the isotope stages based on our resultant timescale of Core MD972143 are well comparable to those of ODP Site 677 by Shackleton *et al.* (1990) (Fig. 5). The difference in $\delta^{18}O$ value between these two curves is typically ~0.6‰, which may be attributed to using different benthic foraminiferal species. While our record is solely based on C. *wuellerstorfi*, the record of Site 677 was obtained from *Uvigerina* spp. Their $\delta^{18}O$ values can be adjusted to those of C. *wuellerstorfi* by subtracting 0.64‰ (Shackleton and Opdyke, 1973). The similarity in the structure of major isotope events among these two time series is more striking for the Pleistocene than for the late Pliocene, when the fluctuations of glacial-interglacial are generally small. The age error associated with the orbitally tuning technique is estimated to be ±5 kyr (Martinson *et al.*, 1987).

Back to about 620 ka, our results of age interpolation down to Stage 16 are similar to those of the SPECMAP timescale (Imbrie *et al.*, 1984). Prior to 620 ka, Shackleton *et al.*'s (1990) new match between the isotope record and the orbital models for isotope stages 17-19, 21, and 35 resulted in older stage ages than those initially given by Ruddiman *et al.* (1986, 1989) and Raymo *et al.* (1989). This revised orbitally derived timescale estimated ages for the last six

major reversals of the Earths magnetic field that are 5-7% older than previously accepted K/Ar-dated magnetic boundaries of Berggren *et al.* (1985). Evidence for older reversal ages have since come from more advanced $^{40}Ar/^{39}Ar$ dating of the Brunhes at 783 ka (Baksi *et al.*, 1992), from the upper Jaramillo boundary at 0.99 Ma (Tauxe *et al.*, 1992), from the base of the Olduvai subchron at 1.98 Ma (Walter *et al.*, 1991) and from the Réunions event at 2.14 Ma (Baksi *et al.*, 1993).

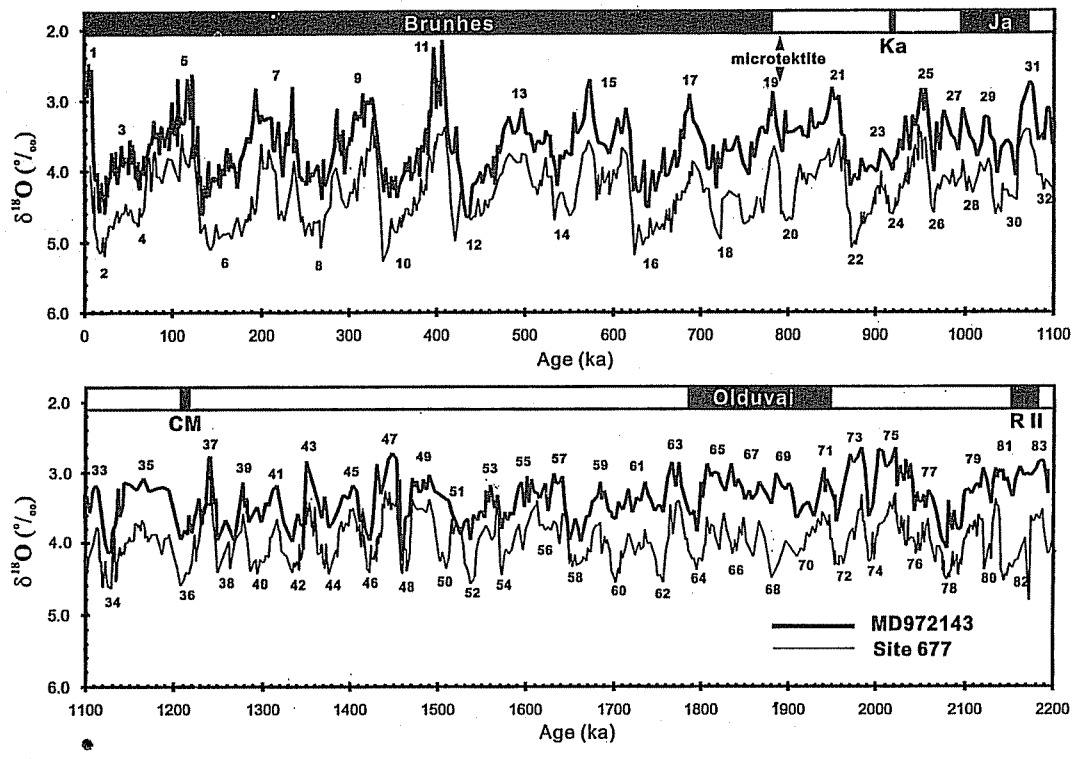

Figure 5. Comparison between the $\delta^{18}O$ records for Core MD972143 and ODP Site 677 (Shackleton et al., 1990) for the past 2.2 Myr. The ages of the major geomagnetic reversals designated in Horng (2000) are calibrated against our newly generated astronomical timescale on the upper bar. Ja, Ka, CM, and RII refer to Jaramillo subchron, and Kamikatura, Cobb Mountain and Réunions II events, respectively.

Noteworthy, no magnetostratigraphy was available at Site 677, and the positions of the major polarity reversals were inferred by biostratigraphic datum levels and the distinctive features of the oxygen isotope record. It is not absolutely certain whether such a composite record is complete. Armed with the detailed magnetostratigraphy in Core MD972143 (Horng, 2000), we calibrated directly the ages of these major geomagnetic reversals against our newly generated astronomical timescale as shown in Figure 5. The estimated ages are well comparable to those radiometric ages previously dated by $^{40}Ar/^{39}Ar$ radiochronological method. This independent

confirmation of Shackleton *et al.*'s (1990) ages implies the completeness and continuity of our record and permits an accurate astronomical calibration.

Mid-Pleistocene Climate Transition

Substantial evidence exists that the $\delta^{18}O$ record from planktonic and benthic foraminifera, primarily a proxy of global ice volume variation, reflects Milankovitch cyclicities. While the individual glacial-interglacial oscillation is tied to the insolation variation caused by orbital forcing, these insolation changes alone cannot account for the long-term cooling observed in geological records. One of the major issues in paleoclimate research has been the explanation of the middle Pleistocene climate shift in the dominant periodicities from the 41- to the 100-kyr cycles (Ruddiman *et al.*, 1986; Berger *et al.*, 1994; Chen *et al.*, 1995; Rutherford and D'Hondt, 2000). After the mid-Pleistocene revolution, the $\delta^{18}O$ record exhibits the dominant 100-kyr "saw-toothed" pattern, whereas isolation time series would predict most of the spectral power to be concentrated at the obliquity and precession bands. A linear response of the climate system to solar insolation changes in the eccentricity band is thought to be insufficient to explain the dominance of the 100-kyr cycle during the late Pleistocene (see review by Imbrie *et al.*, 1993).

The timing and structure of the mid-Pleistocene climate transition and its cause poses one of the most perplexing puzzles of ice-age dynamics.The benthic $\delta^{18}O$ record of the Core MD921743 shows obvious cyclicity throughout the core, which provides a detailed documentation of the timing and magnitude of the global ice-volume variability in the time and frequency domains.As shown in Figure 6, several distinguished features in isotope variability stand out over the past 2.2 Myr. First, the extent of the global ice-volume expanded gradually to its maximum during the Brunhes Chron, while the baseline of the ice-volume remained constant during interglacials. The amplitude of glacial-interglacial fluctuations increased steadily from a mean of about 1‰ or less during the late Pliocene and the early Pleistocene to about 1.8‰ during the late Pleistocene. Prior to 1.5 Ma, ice volume was about 1/2 as large as its full size during the late Pleistocene. Second, the periodicity of glacial-interglacial fluctuations was dominated by the 41-kyr obliquity cycle within the Matuyama Chron, and shifted to the 100-kyr eccentricity cycle within the Brunhes Chron. The mid-Pleistocene climate transition occurred roughly between isotope Stages 25 and 22 and brought forth the first severe glaciation of the late Pleistocene.

For detail, we used band-pass filters to derive the respective 41-kyr and 100-kyr components of the oxygen isotope time series for Core MD972143. The 41-kyr oscillations present a rather simpler pattern than the 100-kyr oscillations. The amplitude of the filtered 41-kyr component remains relatively constant throughout the entire record (Fig. 7a). This indicates that the cyclic changes in the benthic oxygen isotope record responded primarily to high-latitude obliquity forcing associated with a repeated glacial expansion and deepwater formation at the 41-kyr rhythm. In contrast, the strength profile of the filtered 100-kyr band displays interesting secular variations (Fig. 7b).A close-up examination of the filtered record shows that the first high-amplitude 100-kyr cycle began at about 1.2 Ma. Before then, the 100-kyr cycles occurred but were not sustained. Their amplitude remains constant from 1.2 to 0.9 Ma, and then began to increase progressively. The fluctuations of northern hemispheric ice sheets began to show the predominant 100-kyr "saw-toothed" pattern around 700 ka and achieved their full amplitudes at ~400 ka. Our result suggests that the occurrence and evolution of the 100-kyr cycles are of multi-steps, not simply gradual or abrupt.

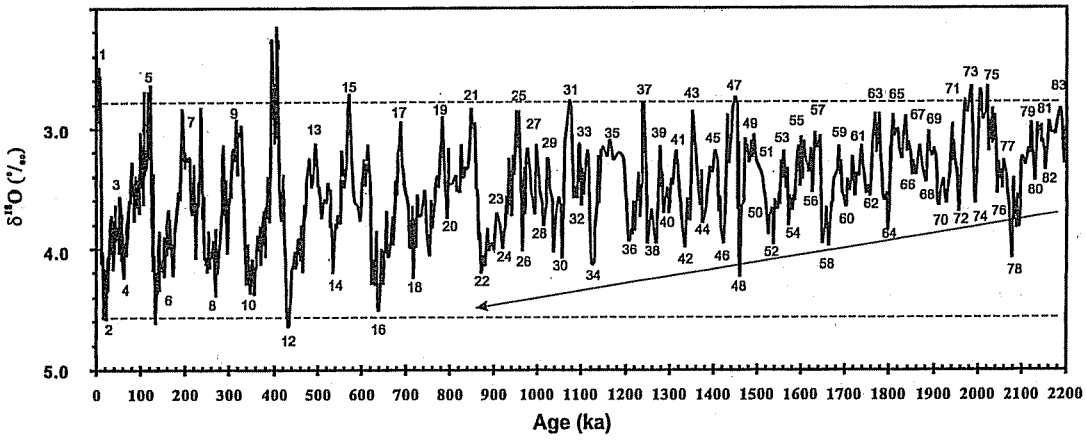

Figure 6. $\delta^{18}O$ of benthic foraminifera *Cibicidoides wuellerstorfi* plotted versus age of Core MD972143. Two reference lines mark the mean $\delta^{18}O$ values of the Holocene and the Last Glacial Maximum.

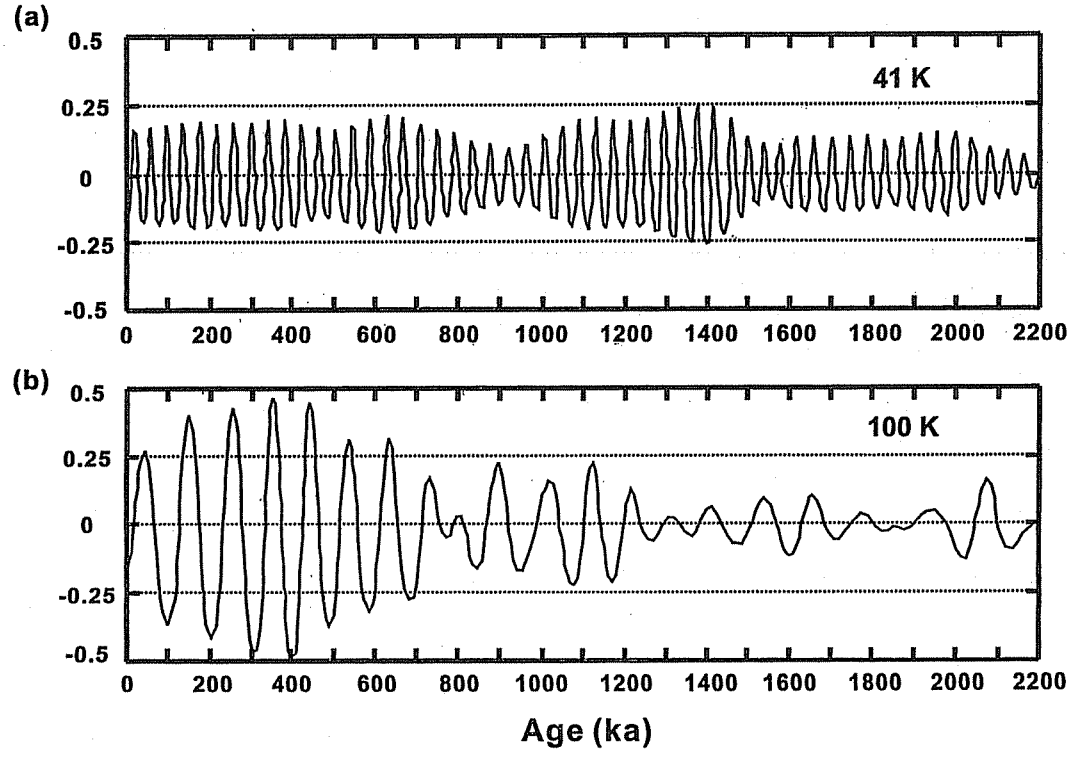

Figure 7. Plots of filtered 41-kyr (a) and 100-kyr cycles (b) from $\delta^{18}O$ data. The filtering was carried out with band-pass filters to derive the respective 100-kyr and 41-kyr components of the MD972143 oxygen isotope time series.

CONCLUSIONS

High-resolution benthic oxygen isotope from Core MD972143 allows us to present the most complete Quaternary record available for the western Pacific Ocean back to 2.2 Ma. The resultant time series provides a detailed documentation of timing and magnitude of global ice volume variability in the time domain and the frequency domain. Several distinguished features are significant. First, the amplitude of glacial-interglacial fluctuations increased steadily from a mean of about 1‰ or less during late Pliocene and early Pleistocene to about 1.8‰ during late Pleistocene. Second, the extent of global ice-volume expanded gradually to its maximum during the Brunhes Chron, while the baseline of ice-volume remained constantly during interglacials. Third, the periodicity of glacial-interglacial fluctuations was dominant by high frequency band (obliquity, 41-kyr cycle) within the Matuyama Chron, and changed to lower frequency band (eccentricity, 100-kyr cycle) within the Brunhes Chron. Fourth, the occurrence and evolution of the 100-kyr cycles display multiple step transitions, not simply gradual or abrupt.

ACKNOWLEDGMENTS

This study is a contribution to the Taiwan IMAGES Program. Special thanks are extended to Dr. Min-Te Chen for his instruction on conducting time-series analyses presented. We thank the scientific party and crew of the IMAGES-III-IPHIS-Leg II Cruise for a successful coring and scientific venture. The support offered by the French MENRT, TAFF, CNRS/INSU and IFRTP to the operation of the cruise vessel Marion Dufrense and the IMAGES Program is highly appreciated. This study has been supported by Grant NSC-90-2116-M002-019 to KYW and YGC. For curation of cores and sampling service, we acknowledge the Core Laboratory located at the National Ocean Science University, funded by the Center of Ocean Research, National Science Council, ROC.

REFERENCES

Bassinot, F.C., Labeyrie, L.D., Vicent, E., Quidelleur, X., Shackleton, N.J. and Lancelot, Y. (1994) The astronomical theory of climate and the age of the Brunhes-Matuyama magnetic reversal: *Earth Planet. Sci. Lett.*, **126**, 91-108.

Baksi, A.K., Hsu, V., McWilliams, M.O. and Farrar, E. (1992) $^{40}Ar/^{39}Ar$ dating of the Brunhes-Matuyama geomagnetic field reversal: *Science*, **256**, 356-357.

Baksi, A.K., Hoffman, K.A. and McWilliams, M. (1993) Testing the accuracy of the geomagnetic polarity time-scale (GPTS) at 2-5 Ma, utilizing $^{40}Ar/^{39}Ar$ incremental heating data on whole-rock basalts: *Earth Planet. Sci. Lett.*, **118**, 135-144.

Berger, A. and Loutre, M.F. (1991) Insolation values for the climate of the last 10 million years: *Quaternary Sci. Rev.*, **10**, 297-317.

Berger, W.H. and Johnson, T.C. (1976) Deep-sea carbonates: dissolution and mass wasting on Ontong-Java Plateau: *Science*, **192**, 785-787.

Berger, W.H., Bonneau, M.-C. and Parker, F.L. (1982) Foraminifera on the deep-sea floor: Lysocline and dissolution rate: *Oceanol. Acta*, **5**, 249-258.

Berger, W.H., Bickert, T., Schmidt, H., Wefer, G. and Yasuda, M. (1993) Quaternary oxygen isotope record of pelagic foraminifers: Site 806, Ontong Java Plateau: *Proc. ODP Sci. Results*, **130**, 381-395.

Berger, W.H., Yasuda, M.K., Bickert, T., Wefer, G. and Takayama, T. (1994) Quaternary time scale for the Ontong Java Plateau: Milankovitch template for Ocean Drilling Program Site 806: *Geology*, **22**, 463-467.

Berggren, W.A., Kent, D.V. and Van Couvering, J.A. (1985) Neogene geochronology and chronostratigraphy, in "*The Chronology of the Geological Record*", edited by Snelling, 211-250, Geological Society of London, Memoir, 10, Oxford, Blackwell.

Berggren, W.A., Kent, D.V. Kent, Swisher III, C.C. and Aubry, M.P. (1995) A revised Cenozoic geochronology and chronostratigraphy, in "*Geochronology, Time Scales and Global Stratigraphic Correlation*", edited by W.A. Berggren, *et al.*, *Spec. Publ. Soc. Econ. Paleontol. Mineral.*, **54**, 129-212.

Chen, J., Farrell, J.W., Murray, D. and Prell, W.L. (1995) Timescale and paleoceanographic implications of a 3.6 m.y. oxygen isotope record from the northeast Indian Ocean (Ocean Frilling Program site 758): *Paleoceanography*, **10**, 21-47.

Curry, W.B., Crowley, T.J. (1987) The $\delta^{13}C$ of equatorial Atlantic surface waters: Implications for ice age pCO_2 levels: *Paleoceanography*, **2**, 489-517.

Curry, W.B., Duplessy, J.C., Labeyrie, L.D. and Shackleton, N.J. (1988) Changes in the distribution of $\delta^{13}C$ of deep water ΣCO_2 between the last glaciation and the Holocene: *Paleoceanography*, **3**, 317-341.

Emiliani, C. (1955) Paleistocene temperatures: *J. Geol.*, **63**, 538-578.

Hagelberg, T., Pisias, N.G. and Elgar, S. (1991) Linear and nonlinear couplings between orbital forcing and the marine $\delta^{18}O$ record during the late Neogene: *Paleoceanography*, **6**, 729-746.

Hays, J.D., Imbrie, J. and Shackleton, N.J. (1976) Variations in the Earth's orbit: Pacemaker of the ice age: *Science*, **194**, 1121-1132.

Herguera, J.C., Jansen, E. and Berger, W.H. (1992) Evidence for a bathyal front at 2000m depth in the glacial Pacific, based on a depth transect on Ontong Java Plateau: *Paleoceanography*, **7**, 273-288.

Horng, C.-S. (2000) Magnetostratigraphic record of IMAGES core MD972143 from the Benham Rise of the western Philippine Sea: *J. Geol. Soc. China*, **43**, 409-422.

Imbrie, J. and Imbrie, J.Z. (1980) Modeling the climatic response to orbital variations: *Science*, **207**, 943-953.

Imbrie, J., Hays, J.D., Martison, D.G., McIntyre, A., Mix, A., Morly, J.J., Pisias, N.G., Prell, W. and Shackleton, N.J. (1984) The orbital theory of Pleistocene climate: support from a revised chronology of the marine $\delta^{18}O$ record, in "*Milankovitch and Climate*", edited by Berger, A., Imbrie, J., Hays, J. D., Kukla, G. and Salzman, B., 269-305, D. Riedel, Norwell, Mass.

Imbrie, J. *et al.* (1992) On the structure and origin of major glaciation cycles, 1, Linear responses to Milankpvitch forcing: *Paleoceanography*, **7**, 701-738.

Imbrie, J. *et al.* (1993) On the structure and origin of major glaciation cycles, 2, The 100,000 years cycle: *Paleoceanography*, **8**, 699-735.

Ingle, J.C., D.E. Kraig, A.H. Bouma and others (1975) Site 292: *Init. Reports DSDP Project*, **31**, 67-82.

Jian, Z., Wang, P., Chen, M.-P., Li, B., Zhao, Q., Buhring, C., Laj, C., Lin, H.L., Pflaumann, U., Bian, Y., Wang, R. and Cheng, X. (2000) Foraminiferal responses to major Pleistocene paleoceanographic changes in the southern South China Sea: *Paleoceanography*, **15**, 229-243.

Keigwin, L. D. (1998) Glacial-age hydrography of the far northwest Pacific Ocean: *Paleoceanography*, **14**, 323-339.

Kent, D.V. (1999) Orbital tuning of geomagnetic polarity time-scales: *Phil. Trans. R. Soc. Lond. A*, **357**, 1995-2007.

Lee, M.-Y. and Wei, K.-Y. (2000) Australasian microtektites in the South China Sea and the West Philippine Sea: Implications for age, size, and location of the impact crater: *Meteor. Planet. Sci.*, **35**, 1151-1155.

Mankinen, E.A., and Dalrymple, G.B. (1979) Revised geomagnetic polarity time scale for the interval 0-5 m.y. B.P.: *J. Geophys, Res.*, **84**, 615-626.

Martinson, D.G., Pisias, N., Hays, J.D., Imbrie, J., Moose, T.C. and Shackleton, N.J. (1987) Age dating and the orbital theory of the ice ages: Development of a high-resolution 0 to 300,000-year chronostratigraphy: *Quat. Res.*, **27**, 1-30.

Ohkouchi, N., Kawahata, H., Murayama. M., Okada, M., Nakamura, T. and Taira, A. (1994) Was deep water formed in the North Pacific during the late Quaternary? Cadmium evidence from the northwest Pacific: *Earth. Planet. Sci. Lett.*, **124**, 185-194.

Raymo, M.E., Ruddiman, W.F., Backman, J., Clement, B.M. and Martinson, D.G. (1989) Late Pliocene variations in northern hemisphere ice sheers and North Atlantic deep water circulation: *Paleoceanography*, **4**, 413-446.

Ruddiman, W.F., McIntyre, A. and Raymo, M.E. (1986) Matuyama 41,000-year cycles: North Atlantic Ocean and northern hemisphere ice sheets: *Earth Planet. Sci, Lett.*, **80**, 117-129.

Ruddiman, W.F., Raymo, M.E., Martinson, D.G., Clement, B.M. and Backman, J. (1989) Pleistocene evolution of Northern Hemisphere climate: *Paleoceanography*, **4**, 353-412.

Rutherford, S. and D'Hondt, S. (2000) Early onset and tropical forcing of 100,000-year Pleistocene glacial cycles: *Nature*, **408**, 72-75.

Schneider, D.A., Kent, D.V. and Mello, G.A. (1992) A detailed chronology of the Australasian impact event, the Brunhes-Matuyama geomagnetic polarity reversal, and global climate change: *Earth Planet. Sci. Lett.*, **111**, 395-405.

Shackleton, N.J. and Opdyke, N.D. (1973) Oxygen isotope and paleomagnetic stratigraphy of equatorial Pacific core V28-238: oxygen isotope temperatures and ice volumes on a 10^5 and 10^6 year scale: *Quat. Res.*, **3**, 39-55.

Shackleton, N.J. and Opdyke, N.D. (1976) Oxygen-isotope and paleomagnetic stratigraphy of Pacific Core V28-239: Late Pliocene to Latest Pleistocene: *Geol. Soc. Am. Mem.*, **145**, 449-464.

Shackleton, N.J., Imbrie, J. and Hall, M.A. (1983) Oxygen and carbon isotope record of east Pacific Core V19-30: Implications for the formation of deep water in late Pleistocene North Atlantic: *Earth Planet. Sci. Lett.*, **65**, 233-244.

Shackleton, N.J., Berger, A. and Peltier, W. (1990) An alternative astronomical calibration of the lower Pleistocene timescale based on ODP Site 677: Trans. R. Soc. Edinburgh: *Earth Sci.*, **81**, 251-261.

Shackleton, N.J., Crowhurst, S., Hagelberg, T., Pisias, N.G. and Schneider, D.A. (1995) A new Neogene time scale: application to LEG 138 sites: *Proc. ODP Sci. Results*, **138**, 73-101.

Smit, J., van Eijden, A.J.M. and Troelstra, S.R. (1991) Analysis of the Australasian microtektite event, the Toba lake event, and the Cretaceous/Paleogene boundary, eastern Indian Ocean: *Proc. ODP Sci. Results*, **121**, 489-503.

Spell, T.L. and McDougall, I. (1992) Revisions to the age of the Brunhes-Matuyama boundary and the Pleistocene geomagnetic polarity timescale: *Geophys. Res. Lett.*, **19**, 1181-1184.

Tauxe, L., Deino, A.D., Behresmeyer, A.K. and Potts, R. (1992) Pinning down the Brunhes/Matuyama and upper Jaramillo boundaries reconciliation of orbital and isotope time scale: *Earth Planet. Sci. Lett.*, **109**, 561-572.

Walter, R.C., Manega, P.C., Hay, R.L., Drake, R.E. and Curtis, G.H. (1991) Laser-fusion $^{40}Ar/^{39}Ar$ dating of Bed I, Olduvai Gorge, Tanzania: *Nature*, **354**, 145-149.

Wei, K.-Y., T.-Q. Lee, and the Shipboard Scientific Party of IMAGESIII/MD106-IPHIS Cruise (Leg II) (1998) Nannofossil biochronology of tephra layers in core MD972143, Benham Rise, Western Philippine Sea: *TAO*, **9**, 153-163.

Wu, G., Herguera, J.C. and Berger, W.H. (1990) Differential dissolution: Modification of late Pleistocene oxygen isotope records in the western equatorial Pacific: *Paleoceanography*, **5**, 581-594.